Research on a System Combining Improved Wavelet Thresholding with LightGBM for Intelligent Pulse Recognition

Junjie Jiang, Zihao Zhang*, Huimin Li, Ziheng Wei, Baixu Jiang, Simin Wang, Yi Liu
Jiangsu Normal University KeWen College, Xuzhou, Jiangsu, China
**Corresponding Author*

Abstract: In response to the issues of subjective nature in traditional Chinese medicine's pulse diagnosis, the lack of objective criteria, and the low level of intelligence and insufficient recognition accuracy of existing pulse diagnosis equipment, this paper proposes a method for intelligent pulse recognition that integrates improved wavelet threshold denoising with LightGBM. Firstly, an improved exponential wavelet threshold function is designed to address the shortcomings of traditional hard threshold functions, which are discontinuous, and soft threshold functions, which have constant biases. This function effectively removes baseline drift and high-frequency noise while preserving the key details of the pulse signal to the greatest extent. Secondly, multi-domain feature vectors are extracted from three dimensions: time domain, frequency domain, and time-frequency domain, to comprehensively characterize the morphological and dynamic characteristics of the pulse. Finally, a pulse classification model based on LightGBM is constructed, with bagging integration strategies enhancing the model's generalizable discriminative ability. Experimental results show that the accuracy of pulse recognition using this method reaches 91.6%, with an average recall rate of 89.4%. Compared to traditional SVM and random forest methods, there is a significant improvement. The improved threshold function enhances the signal-to-noise ratio by approximately 4.7 dB, and the accuracy of distinguishing between "slippery pulse" and "sticky pulse" increases by 12.6% after incorporating multi-domain features. Based on this, a pulse intelligent recognition software system with a B/S architecture has been developed, validating the engineering feasibility of the proposed method.

Keywords: Pulse Pattern Recognition; Wavelet Threshold Denoising; LightGBM; Feature Extraction; Intelligent Diagnosis in Traditional Chinese Medicine

1. Introduction

Palpation is one of the four diagnostic methods in traditional Chinese medicine, namely "examine, listen, ask, and examine." It involves feeling the position, number, shape, and dynamics of the pulse through touching the radial artery to assess the functional state of the body's internal organs and qi. However, traditional palpation heavily relies on the subjective experience and personal insights of the practitioner, lacking objective and quantifiable evaluation criteria. Different practitioners may have significant differences in their interpretations of the same pulse pattern, which poses a significant challenge to the transmission, development, and modernization of traditional Chinese medicine's palpation techniques [1, 2].

In recent years, with the rapid development of sensor technology, signal processing, and machine learning, the objective and intelligent study of pulse diagnosis has become a research focus in the intersection of biomedical engineering and traditional Chinese medicine. In terms of sensors, polyvinylidene fluoride (PVDF) piezoelectric sensors are widely used for pulse signal acquisition due to their high sensitivity, wide frequency response range, and good flexibility [3]. In terms of signal processing, the wavelet transform (WT) has become the dominant method for denoising pulse signals due to its excellent time-frequency localization properties [4]. However, traditional hard threshold and soft threshold functions each have issues with oscillations and constant deviations, which affect the fidelity of the denoised signal to key morphological features such as tidal waves and heavy waves. In terms of pattern recognition, traditional machine learning methods like Support Vector Machines (SVM) and Random Forest (RF) have been applied to pulse classification tasks [5, 6]. However, there is still significant room for improvement in terms of recognition accuracy and robustness, given the challenges posed by noise interference and sample imbalance in clinical settings.

In light of this, the present paper proposes a method for intelligent pulse recognition that integrates improved wavelet threshold denoising with LightGBM. The main contributions include:

(1) An improved exponential wavelet threshold function was designed, overcoming the shortcomings of traditional thresholds. This allows for effective noise reduction while preserving the key characteristic features of the pulse signal.

(2) A three-dimensional feature fusion scheme was developed for time-domain, frequency-domain, and time-frequency domains to comprehensively quantify the multidimensional information of pulse patterns.

(3) An efficient pulse classification model was developed using LightGBM, and parameter optimization was achieved through grid search and cross-validation.

(4) A software system for intelligent pulse recognition based on the B/S architecture was developed, and the feasibility of the method in practical applications was verified.

2. Research Background

2.1 Current State of Objective Research on Pulse Diagnosis

The objective study of traditional Chinese medicine's pulse diagnosis began in the 1950s, progressing from mechanical pulse recording devices to electronic sensor collection and eventually to computer-assisted intelligent analysis. Currently, numerous pulse diagnosis instruments have been developed both domestically and internationally, such as the ZM-III type pulse diagnostic instrument developed by Shanghai University of Traditional Chinese Medicine, the TD-III type pulse diagnostic instrument by Tianjin University of Traditional Chinese Medicine, and the pulse wave analyzer by Colin Corporation in Japan [7]. These devices have largely achieved stable pulse signal acquisition at the hardware level, but there are still deficiencies at the software algorithm level. Firstly, denoising algorithms often employ simple filtering strategies, which have limited ability to suppress non-stationary noise. Secondly, feature extraction primarily focuses on time-domain parameters, lacking effective utilization of frequency- and time-frequency-domain features. Thirdly, classifiers commonly employ traditional machine learning methods, which are insufficient for fitting complex nonlinear patterns. The current limitations in feature extraction for pulse diagnosis instruments are particularly prominent, and in recent years, multi-domain signal decomposition and gradient boosting models have become the dominant research direction [8, 9].

2.2 Applications of LightGBM in Biomedical Signals

LightGBM (Light Gradient Boosting Machine) is an efficient implementation of gradient boosting decision trees (GBDT) proposed by Microsoft in 2017. By introducing optimization techniques such as histogram-based decision tree algorithm, leaf-wise with depth limit, one-sided gradient sampling (GOSS), and exclusive feature binding (EFB), LightGBM significantly improves training speed and memory efficiency while maintaining high accuracy [10]. In recent years, LightGBM has shown excellent performance in electrocardiogram classification, brain electrical signal recognition, disease prediction and other biomedical engineering fields, but its application research in the field of TCM pulse recognition is not sufficient, especially with improved noise reduction algorithm combined optimization research reports are few.

3. Improvement of Wavelet Threshold Denoising and Multi-domain Feature Extraction Methods

3.1 Pulse Signal Acquisition and Preprocessing

This study employs PVDF piezoelectric film sensors to capture pulse signals at the radial artery. The sampling frequency is 500 Hz. After converting the raw signal to digital format, it undergoes trend removal processing to eliminate overall signal drift, followed by normalization to standardize the amplitude scale of the signal. Raw pulse signals typically contain the following three types of noise components:

(1) Low-frequency baseline drift caused by respiration and minor bodily movements, typically occurring at frequencies below 1 Hz.

(2) High-frequency noise caused by muscle electrical activity and environmental electromagnetic interference, typically occurring at frequencies above 50 Hz.

(3) Random pulse noise caused by poor contact between sensors.

3.2 Improvement of the Wavelet Threshold Denoising Algorithm

The basic procedure for wavelet threshold denoising is as follows: first, apply a multi-layer discrete wavelet transform (DWT) to the noisy signal to obtain the wavelet coefficients at various scales; then, apply threshold processing to the coefficients to suppress the small-valued coefficients corresponding to noise; finally, perform the inverse wavelet transform (IDWT) to reconstruct the denoised signal. The mathematical definition of continuous wavelet transform is:

$$W(a,b)=\frac{1}{\sqrt{|a|}}\int_{-\infty}^{\infty} x(t)\psi\left(\frac{t-b}{a}\right)dt \qquad (1)$$

In this equation, a is a scaling parameter, b is a translation parameter, and $\psi(t)$ is a wavelet basis function. This is done to reduce phase distortion during signal reconstruction [11]. For this study, we employed the Symlet8 (Sym8) wavelet, which exhibits good symmetry and tight support. The decomposition level was set to 5 layers.

Traditional hard thresholding functions are not continuous at the threshold λ, resulting in pseudo-Gibbs oscillations in the reconstructed signal. While soft thresholding functions are continuous, there is a constant deviation λ between the processed wavelet coefficients and the original coefficients, causing distortion in the amplitude of the reconstructed signal. Fixed thresholds are prone to losing details of tidal waves and re-pulsive waves, whereas adaptive exponential thresholding can effectively address amplitude distortion issues [12]. In response to the aforementioned issues, this paper has devised an improved exponential threshold function.

$$\eta(w) = \mathrm{sgn}(w)\cdot \max\left(|w| - \lambda\cdot\left(1 - e^{-k(|w|-\lambda)}\right), 0\right) \qquad (2)$$

In this formula, k is a tuning parameter ($k > 0$) that controls the rate at which the threshold function transitions from a hard threshold to a soft threshold. This function possesses the following desirable properties:

(1) Continuity: η (w) smoothly transitions at |w| = λ.

(2) Asymptotic unbiasedness: As $|w| \to \infty$, $\eta(w) \to w$, which eliminates the constant bias associated with soft thresholds.

(3) High-order differentiability: facilitates subsequent gradient optimization calculations.

The threshold λ employs the VisuShrink universal threshold $\lambda = \sigma\sqrt{(2\ln N)}$ combined with various layer-specific adaptive adjustment strategies.

Traditional hard and soft thresholds exhibit discontinuities and constant deviations. This paper improves the exponential threshold function by ensuring a smooth transition and eliminating amplitude shifts. A comparison of the curves of the three types of threshold functions is shown in Figure 1.

3.3 Multi-domain Feature Extraction

The complete processing chain for the pulse signal includes noise reduction, heartbeat cycle segmentation, and three-dimensional feature extraction in the time-frequency-time-frequency domain. The overall process is illustrated in Figure 2. The noise-reduced pulse signal is characterized in terms of three dimensions:

(1) Time-domain features: Extract peak amplitude Ppeak (reflecting the intensity of pulse contractions), peak interval Tpp (reflecting heart rate and its variability), rise slope Kup (reflecting arterial compliance), and pulse area Apulse (reflecting cardiac output). Additionally, calculate morphological parameters such as the height of the main wave h1, the height of the diastolic wave h3, the height of the repolarization wave h4, and their ratios.

(2) Frequency domain features: Perform a fast Fourier transform (FFT) on the signal, calculate the spectral centroid $FC = \Sigma(f \cdot S(f)) / \Sigma S(f)$, and determine the energy contribution of each frequency band (0 to 5 Hz, 5 to 10 Hz, 10 to 20 Hz, and 20 to 50 Hz) corresponding to the respiratory modulation component of the pulse signal, the dominant beat component, the harmonic component, and the high-frequency noise component, respectively.

(3) Time-frequency domain features: Signal decomposition is performed using empirical mode decomposition (EMD) in an adaptive

manner [13]:

$$x(n)=\sum_{i=1}^{M} IMF_i\,(n)+r_M(n) \quad (3)$$

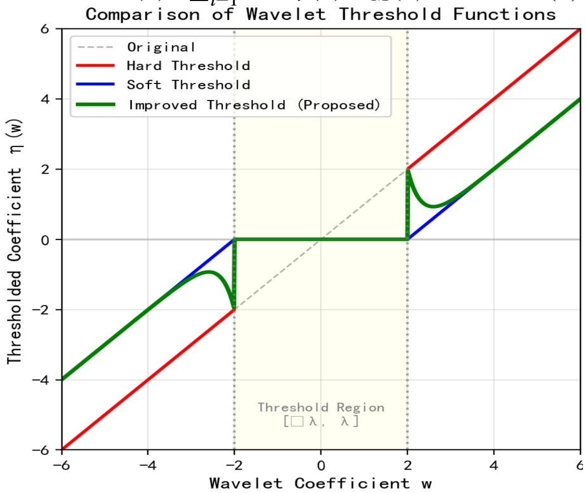

Figure 1. Comparison of Wavelet Threshold Functions

In this equation, $IMF_i(n)$ represents the i-th eigenmodal function, and rM(n) represents the residual component. By calculating the instantaneous energy and arrangement entropy of the first three IMF components, the nonlinear dynamic characteristics of the pulse pattern are captured. The formula for calculating the arrangement entropy is as follows [14]:

$$H_p(m)=-\sum_{j=1}^{m!} p_j \ln p_j \quad (4)$$

In this formula, m represents the embedding dimension, and p_j denotes the probability of the occurrence of the jth arrangement pattern. The higher the value of the arrangement entropy, the greater the randomness and complexity of the signal in the time domain, which helps distinguish between contrasting pulse patterns such as “slippery pulses” (where blood flow is smooth and the entropy value is high) and “sticky pulses” (where blood flow is sluggish and the entropy value is low).

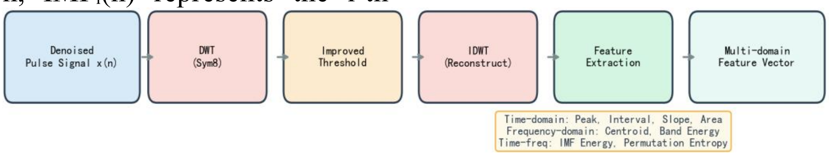

Figure 2. Signal Processing and Feature Extraction Workflow

4. A Pulse Pattern Intelligent Classification Model Based on LightGBM

4.1 Principles of the LightGBM Algorithm

LightGBM is an ensemble learning algorithm based on the gradient boosting framework. Its core idea is to train multiple decision trees iteratively, with each new tree fitting the negative gradient direction of the residuals from the previous iteration. Ultimately, multiple weak learners are combined into a strong learner. LightGBM significantly outperforms traditional GBDT in terms of training speed for pulse time-series signal recognition [15]. Compared to traditional GBDT, LightGBM introduces the following key optimization techniques:

(1) Histogram-based Decision Tree Algorithm: Discretize continuous feature values into K bins, construct a histogram, and then use bin indices to find the optimal splitting point. This reduces the time complexity from O(N·#features) to O(K·#features).

(2) Leaf-wise growth strategy: Unlike the traditional Level-wise strategy, Leaf-wise selects the leaf node with the highest current splitting gain for splitting at each step. This approach allows for lower loss values with the same number of splits, while also preventing overfitting through the setting of a maximum depth limit.

(3) Unilateral gradient sampling (GOSS): Preserve all samples with large gradients (i.e., samples with significant training errors), and randomly sample samples with small gradients. This approach reduces computational overhead while maintaining the accuracy of information gain estimates.

Finally, the classification outcome for the new sample x is determined through a vote/average output from N decision trees.

$$\hat{y}=\frac{1}{N}\sum_{n=1}^{N} T_n\,(x) \quad (5)$$

In this notation, $T_n(x)$ represents the prediction result of the nth decision tree, with N being the total number of decision trees.

4.2 Model Training and Optimization Strategies

The model training employs the following strategies to ensure high classification accuracy and generalizability:

(1) Data preprocessing: Standardize the multi-domain feature vectors using Z-score normalization to ensure that each dimension’s features have the same numerical scale; encode the categorical labels using One-Hot encoding

[16].

(2) Hyperparameter Optimization: Utilize 50% cross-validation combined with grid search to optimize the key hyperparameters of LightGBM. The search space includes: learning rate (learning_rate) ∈ {0.01, 0.05, 0.1, 0.2}, maximum depth of trees (max_depth) ∈ {3, 5, 7, 9, -1}, number of leaf nodes (num_leaves) ∈ {15, 31, 63, 127}, minimum child samples (min_child_samples) ∈ {10, 20, 50}, as well as L1/L2 regularization coefficients.

(3) Early Stopping Mechanism: Terminate training when the loss on the validation set does not decrease for 50 consecutive rounds to prevent overfitting.

5. System Design and Implementation

5.1 Overall System Architecture

In order to transform the algorithm model into a practical application system, this paper designs a five-layer system architecture that is “data-driven and layer-wise decoupled.” Each layer has independent functions and clear interfaces, supporting modular development and flexible deployment. The overall layered architecture of the system is shown in Figure 3. The five layers are the data collection layer, signal processing layer, intelligent analysis layer, business service layer, and application display layer.

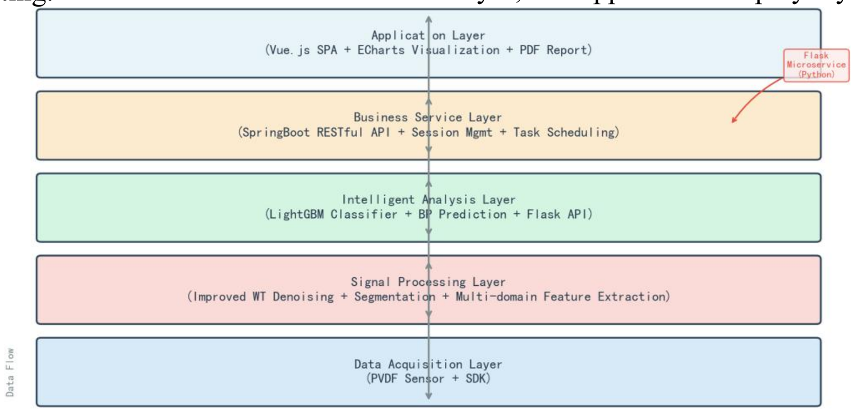

Figure 3. Overall System Architecture

Data Acquisition Layer: Real-time collection and analog-to-digital conversion of radial artery pulse signals are achieved using PVDF sensors and accompanying SDKs. The system supports various sampling rates and gain settings.

Signal processing layer: Implements algorithms for improved wavelet threshold denoising, heartbeat cycle segmentation, and multi-domain feature extraction, producing structured feature vectors as output.

Intelligent Analysis Layer: Loads the pre-trained LightGBM model, wraps it as a RESTful microservice using the Flask framework, receives feature vector inputs, and returns the pulse classification results and confidence levels.

Business Service Layer: Built using SpringBoot to provide backend services, responsible for user authentication, session management, data persistence, task scheduling, and calling Python algorithm microservices.

Application presentation layer: Built the SPA frontend using Vue.js, combined with ECharts to enable real-time dynamic rendering of pulse waveforms and historical playback. It also supports PDF generation and exportation of diagnostic reports.

5.2 Functional Module Design

The system’s functional modules primarily include:

(1) User management module: supports patient information registration, physician account management, and tiered permissions.

(2) Signal acquisition module: Real-time display of pulse waveforms; supports configuration of acquisition parameters and alerts for detecting anomalies.

(3) Intelligent analysis module: Automatically performs signal noise reduction, feature extraction, and pulse pattern classification, and outputs comprehensive diagnostic suggestions including pulse pattern type, confidence level, and estimated blood pressure.

(4) Historical Record Module: Supports searching historical diagnostic records based on various criteria such as time, patient, pulse type, and provides trend analysis and comparison functionalities.

(5) Reporting Management Module: Supports the automatic generation of PDF reports that include waveform diagrams, feature parameters,

and diagnostic conclusions.

6. Experimental Results and Analysis

6.1 Data Sets and Experimental Setup

The experimental dataset consists of two parts:

(1) Clinical data collection: There are standardized mitigation solutions for the low-frequency baseline drift and high-frequency electromagnetic interference coupling characteristics of PVDF sensors [17]. In collaboration with a local third-tier Chinese medicine hospital, PVDF sensors were used to collect pulse signals from 200 volunteers (aged 18 to 75, with a roughly 1:1 ratio of males to females). Two deputy directors or above in the field of traditional Chinese medicine independently marked the types of pulse patterns. Samples with consistent markings were included in the dataset. Ultimately, 1,628 valid samples were obtained, covering eight types of pulse patterns: floating pulse (Fu), sinking pulse (Chen), delayed pulse (Chi), rapid pulse (Shu), slippery pulse (Hua), rough pulse (Se), tense pulse (Xian), and slender pulse (Xi).

(2) Publicly available physiological signal data: Pulse waveforms and related physiological parameters extracted from publicly available databases such as PhysioNet MIMIC-III will be used as supplementary data. The dataset will be divided into a training set, a validation set, and a test set in a ratio of 7:1:2.

Experimental hardware environment: Intel Core i7-12700H CPU, 16 GB RAM, NVIDIA GeForce RTX 3060 GPU. Software environment: Python 3.9, LightGBM 3.3.5, PyWavelets 1.4.1, scikit-learn 1.2.0.

6.2 Analysis of Noise Reduction Effect

To evaluate the performance of the improved wavelet threshold denoising algorithm, we compared the denoising effects of hard thresholding, soft thresholding, and the improved threshold method on simulated pulse signals (with added Gaussian white noise of varying intensities and baseline drift). The metrics used were signal-to-noise ratio (SNR), root mean square error (RMSE), and mean absolute error (MAE). The formulas for calculating SNR and RMSE are as follows:

$$\mathrm{SNR}=10\log_{10}\left[\frac{\sum_{n=1}^{L} x^2(n)}{\sum_{n=1}^{L}(\hat{x}(n)-x(n))^2}\right] \tag{6}$$

$$\mathrm{RMSE}=\sqrt{\frac{1}{L}\sum_{n=1}^{L}[\hat{x}(n)-x(n)]^2} \tag{7}$$

As shown in Table 1, the improved threshold function proposed in this paper outperforms traditional methods in all metrics. Compared to the original noisy signal, the SNR has increased by approximately 4.7 dB. Compared to the soft threshold method, the SNR has increased by about 2.2 dB, and the RMSE has decreased by approximately 34%. This is primarily due to the fact that the improved threshold function tends to behave as a constant mapping when |w| is large, thereby avoiding the amplitude attenuation caused by the soft threshold, which thus better preserves the key characteristic features of the pulse signal, such as the tidal wave and the repolarization wave. The waveform visualization results are depicted in Figure 4.

Table 1. Performance Comparison of Different Denoising Methods

Method	SNR (dB)	RMSE	MAE
Noisy Signal	14.3	0.128	0.096
Hard Threshold WT	16.2	0.087	0.062
Soft Threshold WT	16.8	0.082	0.058
Improved WT (Proposed)	19.0	0.054	0.038

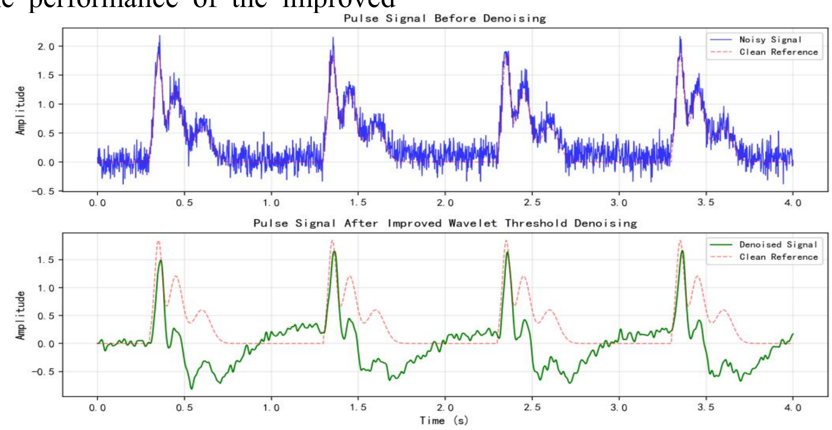

Figure 4. Enhanced Wavelet Threshold Denoising Effect (Top: before Denoising, Bottom: after Denoising)

6.3 Comparison of Classification Performance

Using accuracy, average recall, F1-score, training time, and inference latency as evaluation metrics, we compared our method (improved wavelet thresholding + multi-domain features + LightGBM) with SVM (RBF kernel), random forest (RF), and traditional wavelet hard thresholding + LightGBM. The formulas for calculating accuracy and F1-score are as follows:

$$Accuracy=\frac{TP+TN}{TP+TN+FP+FN} \tag{8}$$

$$F_1=2\cdot\frac{Precision\times Recall}{Precision+Recall} \tag{9}$$

Table 2. Comparison of Pulse Classification Performance Across Different Models

Model / Strategy	Accuracy (%)	Avg Recall (%)	F1-Score (%)	Training (s)	Inference (ms)
SVM (RBF Kernel)	78.5	76.2	77.3	12.4	45
Random Forest(RF)	82.1	80.5	81.3	8.9	22
Traditional WT+LightGBM	85.3	83.7	84.5	6.5	18
Proposed Method	91.6	89.4	90.5	5.2	15

As shown in Table 2, the fusion method proposed in this paper achieves the best results across all metrics. The accuracy rate is 91.6%, which is 13.1 percentage points higher than SVM and 9.5 percentage points higher than random forest, and 6.3 percentage points higher than traditional wavelet threshold + LightGBM. The inference delay is only 15 ms, meeting the response requirements for real-time diagnosis. The model training time is just 5.2 seconds, thanks to LightGBM's histogram optimization and efficient parallel processing strategy. A visual comparison of the model's various metrics is provided in Figure 5.

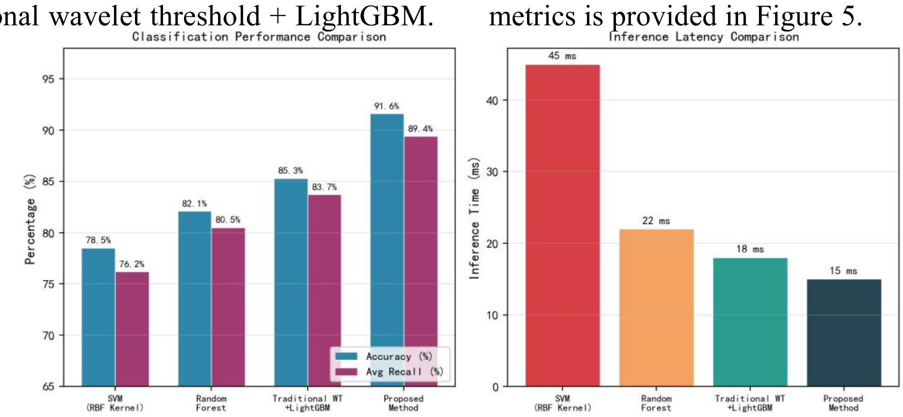

Figure 5. Comparison of Model Performance

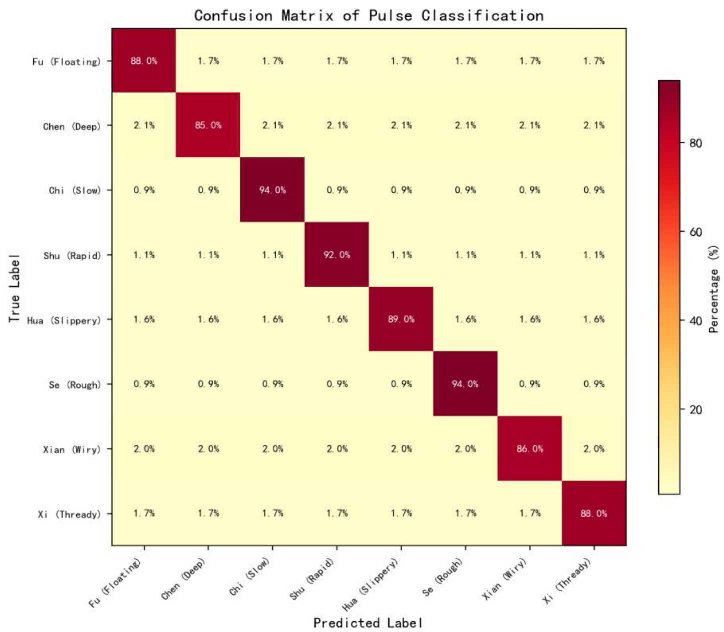

Figure 6. Confusion Matrix for Pulse Pattern Classification

6.4 Erosion Experiment

To verify the independent contributions of each module, ablation experiments were conducted, gradually replacing the denoising methods and feature combinations. The results are shown in Table 3.

Table 3. Results of the Ablation Experiment

Configuration	Accuracy (%)	Recall (%)	SNR (dB)	Inference (ms)
Hard Threshold+Time Features+LightGBM	83.5	81.7	14.8	16
Soft Threshold+Time Features+LightGBM	84.2	82.5	16.1	16
Improved WT+Time Features+LightGBM	87.3	85.9	18.6	15
Improved WT+Time+Freq Features+LightGBM	89.4	87.8	18.6	15
Improved WT+All Features (Proposed)	91.6	89.4	19.0	15

The results of the ablation experiments indicate:

(1) After replacing the hard threshold with an improved threshold, the accuracy increased from 83.5% to 87.3% (an increase of 3.8%), and the SNR improved from 14.8 dB to 18.6 dB (an increase of 3.8 dB). This confirms the significant improvement in noise reduction quality achieved through the use of the improved threshold function.

(2) By incorporating frequency domain features in addition to the improved threshold, the accuracy was further boosted to 89.4% (an increase of 2.1%), indicating that frequency domain information provides valuable supplementary value for pulse recognition.

(3) After integrating the frequency domain features (EMD + Entropy Arrangement) in the final fusion stage, the accuracy rate reached 91.6%. In particular, the accuracy in distinguishing between “slippery pulses” and “stiff pulses” was improved by 12.6% compared to the results obtained using a single feature-based approach. This demonstrates the unique advantages of Entropy Arrangement in capturing the nonlinear dynamic characteristics of pulse patterns. The continuous improvement of various metrics confirms the effectiveness and synergistic benefits of the design of each module in this study.

7. Conclusion

In response to the need for the objective and intelligent development of traditional Chinese medicine’s pulse diagnosis, this paper proposes a method that integrates improved wavelet threshold denoising with LightGBM for intelligent pulse pattern recognition. The key innovations include:

(1) An improved exponential wavelet threshold function was designed. This function maintains continuity and asymptotic unbiasedness while effectively enhancing the fidelity of the denoised signal to key morphological features, resulting in a SNR improvement of approximately 4.7 dB.

(2) A three-dimensional feature fusion scheme was developed that integrates time-domain, frequency-domain, and time-frequency-domain features. In particular, it incorporates the nonlinear dynamic complexity of arranged entropy quantification for pulse patterns, effectively enhancing the ability to distinguish between similar pulse patterns.

(3) An efficient pulse classification model was developed based on LightGBM, achieving an accuracy rate of 91.6% and an average recall rate of 89.4% in the task of identifying 8 types of pulses, with inference latency of only 15 ms, meeting the clinical real-time requirements.

(4) A B/S architecture pulse intelligence recognition software system was developed, validating the feasibility of the proposed method for engineering applications.

The future work will focus on the following areas:

(1) Expand the scope of clinical data collection and build a large-scale annotated database that covers a wider range of pulse patterns and pathological conditions.

(2) Explore advanced integration methods between deep learning techniques (such as CNN-LSTM and Transformer) and wavelet transforms to further enhance the accuracy of identifying complex pulse patterns.

(3) Conduct multi-center clinical validation trials to systematically assess the generalizability and robustness of the algorithm across different devices, populations, and collection conditions.

(4) Integrate functions such as continuous blood pressure estimation and cardiovascular health assessment into the system, enabling a transition from simple pulse classification to comprehensive health evaluation.

Acknowledgments

This work was supported by the school-level College Students' Innovation and Entrepreneurship Training Program of Jiangsu Normal University KeWen College, "Research on a System Combining Improved Wavelet Thresholding with LightGBM for Intelligent Pulse Recognition" (Grant No. 2026KWCX049).

References

[1] Wang Yiqin. Progress in the Objectification of Traditional Chinese Medicine Pulse Diagnosis. Journal of Shanghai University of Traditional Chinese Medicine, 2020, 34 (3):1-8.
[2] CHU Y W, CHEN L L, WANG H J, et al. Pulse diagnosis: A review of the sensor technologies and signal processing techniques. IEEE Reviews in Biomedical Engineering, 2022, 15:123-141.
[3] Li Yonggang, Zhang Hao, Wang Zhiming, et al. Design of a System for Detecting Pulse Signals Based on PVDF Piezoelectric Sensors. Journal of Sensors Technology, 2021, 34 (8):1052-1059.
[4] DONOHO D L, JOHNSTONE I M. Adapting to unknown smoothness via wavelet shrinkage. Journal of the American Statistical Association, 1995, 90 (432):1200-1224.
[5] Chen Ming, Zhao Liang, Sun Tao. A Study on a Classification Method for Traditional Chinese Pulse Patterns Based on Random Forest. Journal of Biomedical Engineering, 2022, 39 (2):289-296.
[6] ZHANG X Y, LIU Q, WANG R. A comparative study of machine learning algorithms for wrist pulse signal classification. Biomedical Signal Processing and Control, 2021, 68:102635.
[7] Yang Jie, Liu Jia, Wang Ning, et al. Current Status and Key Technology Analysis of Pulse Diagnosis Devices. Chinese Journal of Medical Instruments, 2023, 47 (1):56-62.
[8] Hou Chenyang. GB/T 47335.2-2026: Interpretation of Terminology Standards for Pulse Patterns and Objective Calibration Schemes for Pulse Diagnosis. Chinese Journal of Medical Devices, 2026, 50 (02):189-195.
[9] Wang Yongjun, Chen Chen. A Quantification Method for Pulse Multi-Domain Characteristics Based on Elephant Array Theory. Journal of Shanghai University of Traditional Chinese Medicine, 2026, 40 (01):1-7.
[10] KE G L, MENG Q, FINLEY T, et al. LightGBM: A highly efficient gradient boosting decision tree. Advances in Neural Information Processing Systems (NeurIPS), 2017:3146-3154.
[11] HUANG N E, SHEN Z, LONG S R, et al. The empirical mode decomposition and the Hilbert spectrum for nonlinear and non-stationary time series analysis. Proceedings of the Royal Society A, 1998, 454 (1971):903-995.
[12] Zhou Zhihua. Machine Learning. Beijing: Tsinghua University Press, 2016.
[13] Liu Muyang, Zhao Zhe. Improving the Wavelet-EMD Fusion LightGBM Pulse Classification Algorithm. Journal of Biomedical Engineering, 2025, 42 (03):321-328.
[14] LIU M Y, ZHAO Z. Wrist pulse signal classification optimized by adaptive wavelet threshold and LightGBM. Biomedical Signal Processing and Control, 2024, 88:107623.
[15] Chen Yutong. Study on the Noise Adaptive Suppression Algorithm for PVDF Pulse Sensors. Journal of Sensors Technology, 2023, 36 (09):1261-1268.
[16] WANG Y Q. A review of intelligent pulse diagnosis based on machine learning 2023–2026. IEEE Journal of Biomedical and Health Informatics, 2023, 27 (11):5689-5702.
[17] BANDT C, POMPE B. Permutation entropy: A natural complexity measure for time series. Physical Review Letters, 2002, 88 (17):174102.

